Ultrastrong Light-Matter Coupling Regime with Polariton Dots

Y. Todorov,[1,*] A. M. Andrews,[2] R. Colombelli,[3] S. De Liberato,[1,4] C. Ciuti,[1] P. Klang,[2] G. Strasser,[2] and C. Sirtori[1]

[1]*Laboratoire "Matériaux et Phénomenes Quantiques," Unversité Paris Diderot-Paris 7, CNRS-UMR 7162, 75013 Paris, France*

[2]*Solid State Electronics Institute TU Wien, Floragasse 7, A-1040 Vienna, Austria*

[3]*Institut d'Electronique Fondamentale, Université Paris-Sud and CNRS-UMR 8622, F-91405 Orsay, France*

[4]*Department of Physics, University of Tokyo, Bunkyo-ku, Tokyo 113-0033, Japan*

(Received 16 June 2010; revised manuscript received 8 September 2010; published 2 November 2010)

The regime of ultrastrong light-matter interaction has been investigated theoretically and experimentally, using zero-dimensional electromagnetic resonators coupled with an electronic transition between two confined states of a semiconductor quantum well. We have measured a splitting between the coupled modes that amounts to 48% of the energy transition, the highest ratio ever observed in a light-matter coupled system. Our analysis, based on a microscopic quantum theory, shows that the nonlinear polariton splitting, a signature of this regime, is a dynamical effect arising from the self-interaction of the collective electronic polarization with its own emitted field.

DOI: 10.1103/PhysRevLett.105.196402 PACS numbers: 71.36.+c, 42.50.Pq, 71.45.Gm, 78.67.De

Light-matter interaction in the strong coupling regime is a reversible process in which a photon is absorbed and reemitted by an electronic transition at a rate equal to the coupling energy divided by the Plank constant $\hbar$. This situation is observed in systems where an electronic transition, embedded in an optical cavity, has the same energy as the confined photonic mode [1,2]. An adequate description of the system is given using quantum mechanics that permits description of the stationary states as mixed particles, the polaritons, which are a linear combination of light and matter wave functions [3,4]. Recently, the cavity polaritons produced by the intersubband transitions in a highly doped quantum well have received considerable interest [5–7]. In this system the number of available excitations per unit volume can be very high, and an unexplored limit can be reached where the interaction energy $\hbar\Omega_R$ (Ω_R is the Rabi frequency) is of the same order of magnitude as the transition $\hbar\omega_{12}$, the recently named "ultrastrong coupling regime" [8]. We have developed a microscopic quantum theory and provided experimental evidence linking this regime to the collective phenomena in the confined electronic gas [9]. Our studies are conducted with "polaritons dots" produced using zero-dimensional microcavities. In these systems we have measured an unprecedented ratio $2\Omega_R/\omega_{12} = 0.48$, which is more than twice the highest values reported in the literature [6,7,10]. This high ratio has allowed us to observe the nonlinearities in the coupling constant, which are indisputable features of the ultrastrong coupling regime.

A natural framework to describe the interaction of quantized light with a solid state system is the multipolar coupling Hamiltonian involving the electric displacement $\mathbf{D}(\mathbf{r})$ [11,12], and the local polarization field $\mathbf{P}(\mathbf{r})$ of the optically active excitations [13]. In the case of an intersubband transition of energy $\hbar\omega_{12}$ we can define a polarization operator as $b_{\mathbf{q}}^{\dagger} = 1/\sqrt{N}\sum_{\mathbf{k}} c_{2\mathbf{k}+\mathbf{q}}^{\dagger} c_{1\mathbf{k}}$ where $\mathbf{q}$ is the photon wave vector, $N = N_1 - N_2$ is the population difference between the subbands 1 and 2, and $c_{1\mathbf{k}}$ and $c_{2\mathbf{k}}^{\dagger}$ are the corresponding fermionic destruction or creation operators [8]. Figure 1(a) illustrates a quantum well (QW) of thickness L_{qw} and Fig. 1(b) the schematic principle of the operator $b_{\mathbf{q}}^{\dagger}$ which promotes coherently each electron from the ground subband to the excited one, with an identical probability of $1/\sqrt{N}$. The polarization density is then $\mathbf{P}(z, \mathbf{r}_{\parallel}) = (\hat{\mathbf{z}} d_{12}\sqrt{N}/L_{\mathrm{qw}}S)\sum_{\mathbf{q}}(b_{\mathbf{q}}^{\dagger} + b_{\mathbf{q}})\sqrt{2}\cos(\mathbf{q}.\mathbf{r}_{\parallel})\eta(z)$, where z is the well growth axis, $\hat{\mathbf{z}}$ the corresponding unit vector and $\mathbf{r}_{\parallel} = (x, y)$ the in-plane position [Fig. 1(c)], d_{12} the transition dipole and S the area of the system [14]. The function $\eta(z)$ equals 1 in the quantum well slab and 0 everywhere else. Let the polarization field interact with the fundamental TM mode of 0D square-shaped microcavity of frequency ω_c and dimensions $s \times s \times L_{\mathrm{cav}}$ [Fig. 1(c)]. The electric displacement of this mode is $\mathbf{D}(\mathbf{r}) = \hat{\mathbf{z}} i\sqrt{\varepsilon\varepsilon_0\hbar\omega_c/L_{\mathrm{cav}}S}(a^{\dagger} - a)\cos(\pi y/s)$, with ε the background dielectric constant, and $a^{\dagger}$ the photonic creation operator [15,16]. We have therefore $|\mathbf{q}| = \pi/s$ which is very small compared to the typical electron wave vectors $\mathbf{k}$ and will be neglected in the definition of $b_{\mathbf{q}}^{\dagger}$. In this long wavelength limit the dipole interaction Hamiltonian $H_I = \int d^3r(-\mathbf{D}\cdot\mathbf{P} + \mathbf{P}^2/2)/\varepsilon\varepsilon_0$ [11,12] can be expressed as

$$H_I = i d_{12}\sqrt{\frac{N\hbar\omega_c}{2\varepsilon\varepsilon_0 L_{\mathrm{cav}}S}}(a - a^{\dagger})(b + b^{\dagger}) + \frac{d_{12}^2 N}{\varepsilon\varepsilon_0 L_{\mathrm{qw}}S}(b + b^{\dagger})^2. \quad (1)$$

The quadratic term of (1) describing the polarization self-interaction is usually disregarded, but we are going to show that it plays an important role in the limit of very strong

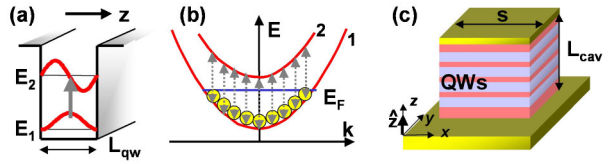

FIG. 1 (color online). (a) Semiconductor quantum well (QW) with two subbands of energies E_1 and E_2. (b) In-plane parabolic dispersion of the energy subbands, with a sketch of the action of the polarization operator $b^\dagger$ (arrows). E_F is the Fermi level. (c) Multiple QWs embedded in a square-shaped microcavity.

light-matter coupling. The notations of the problem can be greatly simplified introducing the plasma frequency ω_P:

$$\omega_P^2 = \frac{e^2 f_{12} N}{m^* \varepsilon \varepsilon_0 L_{\rm qw} S} = \frac{2\omega_{12} d_{12}^2 N}{\hbar \varepsilon \varepsilon_0 L_{\rm qw} S}, \tag{2}$$

where $f_{12} = 2m^*\omega_{12} d_{12}^2/\hbar e^2$ is the oscillator strength, and m^* the effective electron mass [9]. The full Hamiltonian of the system, including the contributions of the cavity and the material excitation is then

$$H = \hbar\omega_c (a^\dagger a + 1/2) + \hbar\omega_{12} b^\dagger b + \frac{i\hbar\omega_P}{2} \times \sqrt{f_w \frac{\omega_c}{\omega_{12}}} (a - a^\dagger)(b + b^\dagger) + \frac{\hbar\omega_P^2}{4\omega_{12}} (b + b^\dagger)^2. \tag{3}$$

Here $f_w = L_{\rm qw}/L_{\rm cav}$ is the overlap factor between the polarization medium and the cavity mode. Clearly, the polarization self-energy depends only on the matter frequencies ω_{12}, ω_P. The matter part $H_{\rm pol} = \hbar\omega_{12} b^\dagger b + \hbar\omega_P^2/4\omega_{12}(b + b^\dagger)^2$ can therefore be diagonalized separately through the Bogoliubov procedure [17], by defining a destruction operator p such that $[p, H_{\rm pol}] = \hbar\tilde{\omega}_{12} p$. This leads to $H_{\rm pol} = \hbar\tilde{\omega}_{12} p^\dagger p$ where

$$\tilde{\omega}_{12} = \sqrt{\omega_{12}^2 + \omega_P^2} \quad \text{and} \quad p = \frac{\tilde{\omega}_{12} + \omega_{12}}{2\sqrt{\tilde{\omega}_{12}\omega_{12}}} b + \frac{\tilde{\omega}_{12} - \omega_{12}}{2\sqrt{\tilde{\omega}_{12}\omega_{12}}} b^\dagger \tag{4}$$

The new polarization eigenfrequency $\tilde{\omega}_{12} = \sqrt{\omega_{12}^2 + \omega_P^2}$ is identical to the result of Ando *et al.* [9], describing the collective oscillations of two-dimensional electrons, an effect known as the "depolarization shift" [18]. This phenomenon appears naturally from the complete interaction Hamiltonian (3) expressed in the Power-Zienau-Woolley (PZW) representation [11].

Moreover, it is remarkable that the coupling with the cavity mode is also proportional to ω_P. Therefore the limit of very strong light-matter interaction also implies a large depolarization shift. Our model allows us to clearly quantify the link between the two features. Using (4) we replace $b^\dagger/b$ by the renormalized polarization operators $p^\dagger/p$, to obtain a linear interaction Hamiltonian:

$$H = \hbar\omega_c (a^\dagger a + 1/2) + \hbar\tilde{\omega}_{12} p^\dagger p + i\frac{\hbar\omega_P}{2} \times \sqrt{f_w \frac{\omega_c}{\tilde{\omega}_{12}}} (a - a^\dagger)(p + p^\dagger). \tag{5}$$

The eigenvalues of (5) are provided by the equation:

$$(\omega^2 - \tilde{\omega}_{12}^2)(\omega^2 - \omega_c^2) = f_w \omega_P^2 \omega_c^2 \tag{6}$$

Equations (5) and (6) describe the coupling between two independent oscillators: the bare microcavity mode and the bosonic excitation renormalized by its own radiated field. Its roots, $\omega_{\rm UP}$ and $\omega_{\rm LP}$ are the frequencies of the two polariton states. Note that the relevant features of the ultrastrong coupling are present through the antiresonant terms $a^\dagger p^\dagger$ and ap. The Hamiltonian (5) can be related to the full standard minimal coupling Hamiltonian used so far for the study of the ultrastrong coupling regime [8], through the inverse PZW transformation [19].

Equation (6), which is the polariton dispersion relation, allows us to introduce an effective dielectric constant through the usual relation $\bar{\varepsilon}(\omega)\omega^2/c^2 = \mathbf{q}^2 = \varepsilon\omega_c^2/c^2$. Identifying $\bar{\varepsilon}(\omega)$ from (6) we find

$$1/\bar{\varepsilon}(\omega) = f_w/\varepsilon_{\rm qw}(\omega) + (1 - f_w)/\varepsilon. \tag{7}$$

Here $\varepsilon_{\rm qw}(\omega) = \varepsilon(1 - \omega_P^2/(\omega^2 - \omega_{12}^2))$ is the usual QW slab dielectric constant [20]. This is precisely the results of Zaluzny *et al.* [21], which confirms the pertinence of our model. Moreover, in the limit $f_w = 1$ we recover the homogeneous Hopfield model [3,4].

Taking the resonant case, $\omega_c = \omega_{12}$, from (6) we can deduce that, up to third order in ω_P/ω_{12}, the polariton splitting is $\omega_{\rm UP} - \omega_{\rm LP} = \sqrt{f_w}\omega_P = 2\Omega_R$. Note that the Rabi frequency Ω_R goes to zero when f_w does it, independently from the value of ω_P. Indeed, by changing the overlap factor in (5) and (6) one can move the system from the ultrastrong coupling regime to the uncoupled situation. Both situations, however, bring the signatures of the plasma frequency ω_P, which appears as the fundamental quantity for the light-coupled 2D electronic system.

To confirm experimentally these effects, it is necessary to have a system with a large ratio ω_P/ω_{12}. This situation is readily obtained for intersubband transition in the THz spectral region using highly doped quantum wells. Our system is composed of a thin $GaAs/Al_{0.15}Ga_{0.85}As$ multiquantum well structure represented in Fig. 2(a). It comprises $N_{\rm qw} = 25$ quantum wells of width $L_{\rm qw} = 32$ nm separated by $L_{\rm bar} = 20$ nm barriers, silicon δ doped with a sheet density of 2×10^{11} cm^{-2}. The intersubband transition energies between the first three subbands are, respectively, $E_{12} = E_2 - E_1 = 12.4$ meV (3 THz) and $E_{32} = E_3 - E_2 = 19.9$ meV (4.8 THz). Light is confined in the vertical direction by a metal plate on one side and a

two-dimensional array of squared metallic pads of size s on the other. In the lateral direction the confinement is provided by the strong impedance mismatch between the regions covered and uncovered by the metal, as shown in Figs. 2(b) [6,15]. This arrangement creates a 0D cavity with a reduced volume with respect to the wavelength of the mode, on the order of $V_{\mathrm{cav}}/\lambda_{\mathrm{res}}^3 = 10^{-4}$. The optical response of the cavities is studied in spectrally resolved reflectometry measurements, at different angles of incidence, using a Bruker Fourier transform infrared spectrometer [15]. In Figs. 2(c) and 2(d) we present two contour plots as a function of the temperature: the absorption of a reference uncoupled system [2(c)] and the reflectivity of a resonantly coupled cavity, $\hbar\omega_c = E_{12}$ [2(d)]. In the reference, the absorption is measured in a multipass configuration using a sample with no cavity. At high temperature electrons are populating several subbands and have a similar density on the fundamental state E_1 and on the first excited state E_2. When the temperature is lowered, the population of E_1 increases with respect to E_2, which allows us to vary $N = N_1 - N_2$ and ω_P. In Fig. 2(c) one can clearly observe the two absorption peaks corresponding to E_{12} and E_{23}. Their intensities have opposite behavior as a function of the temperature, as expected by the electron redistribution on the subbands. Moreover, the E_{12} transition has blue shifted at low temperatures due to the increased electronic density on the ground state, which is the evidence of the depolarization shift.

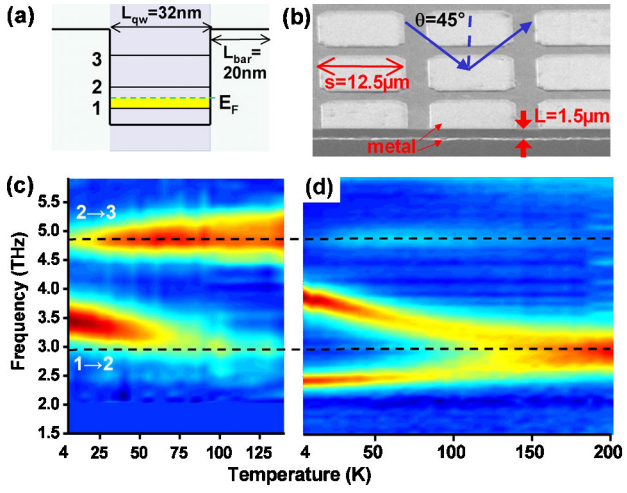

FIG. 2 (color online). (a) Schematics of the QW media of our samples. The first two electronic transitions are $E_2 - E_1 = 12.4$ meV (3 THz) and $E_3 - E_2 = 19.9$ meV (4.8 THz). (b) Electronic microscope image of the cleaved facet of an array of metal-dielectric-metal patch cavities. (c) Contour plot of the QW multipass absorption as a function of the frequency and temperature, revealing the first $1 \rightarrow 2$ and the second $2 \rightarrow 3$ QW transitions. (d) Reflectivity contour plot, with $\theta = 45°$, as a function of frequency and temperature, for a cavity ($s = 12.5$ μm) with $\omega_c = 3$ THz, resonant with the $1 \rightarrow 2$ QW transition.

In Fig. 2(d) the reflectivity peak clearly splits into the upper and lower polariton branches for temperature below 120 K. The separation between the branches keeps increasing down to 4 K, up to a maximum value of 1.41 THz. In the same panel, we can observe also the E_{23} transition that peaks between 60 and 80 K and disappears at 4 K.

Figure 3 presents a detailed characterization of the cavities with different patch widths s. At $T = 300$ K the reflectivity spectra presented in Fig. 3(a) feature only the bare cavity mode allowing us to map its frequency ω_c as a function of $1/s$ (inset). As shown in the inset, ω_c is independent from the incident angle θ, attesting the 0D character of the microcavities [15]. Figure 3(b) summarizes the spectra at $T = 4.5$ K, where the cavity mode is coupled with the fundamental intersubband transition $1 \rightarrow 2$, with a very clear anticrossing behavior. The remarkable feature of our data is the minimum polariton separation, the Rabi splitting, $2\Omega_R = \omega_{\mathrm{UP}} - \omega_{\mathrm{LP}} = 1.41$ THz, which is 48% of the bare intersubband transition $E_{12} = 3$ THz. This value is, to our knowledge, the largest fraction ever measured in a light-matter interacting system. Notice that the typical width of the resonances is in the order of 250 GHz, thus a factor of 5 to 6 less than the Rabi splitting.

In Fig. 4(a) the polariton peak energies (blue dots) for the resonant case [Fig. 2(c)] are plotted as a function of ω_P, which can be easily inferred from the polariton splitting ($2\Omega_R = \sqrt{f_w}\omega_P$) and the knowledge of f_w: for our structure we have $f_w = N_{\mathrm{qw}}L_{\mathrm{qw}}/L_{\mathrm{cav}} = 0.62$. On the same graph, we can therefore plot the $1 \rightarrow 2$ peaks of the uncoupled structure as a function of the temperature, measured from the multipass absorption spectra (red triangles). The solid (blue) lines are the roots of Eq. (6) at resonance

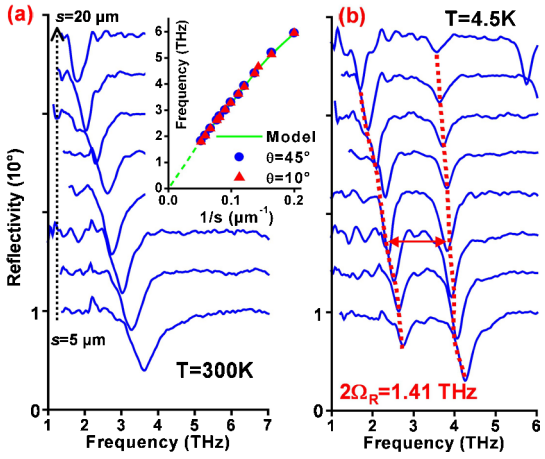

FIG. 3 (color online). (a) Reflectivity spectra for different cavities with decreasing size s, for an incident angle $\theta = 10°$. Spectra have been offset for clarity. The inset summarizes the frequency of the cavity mode as a function of $1/s$ measured at 10° (red triangles) and 45° (blue dots) angles of incidence. (b) Low temperature ($T = 4.5$ K) reflectivity spectra $\theta = 10°$, for the same cavities as in (a). The minimal polariton separation is the Rabi splitting $2\Omega_R = 1.41$ THz.

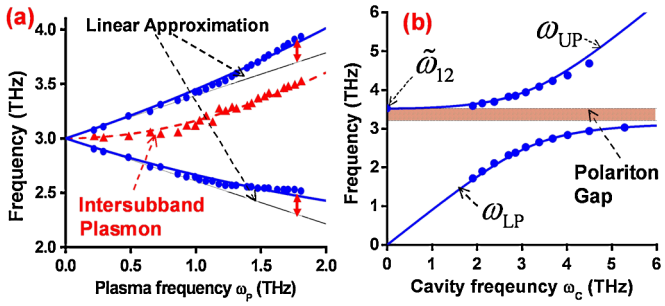

FIG. 4 (color online). (a) The two polariton peaks ω_{UP} and ω_{LP} (in blue) as a function of the plasma frequency ω_P, in the resonant case $\omega_c = \omega_{12}$. We have also plotted the energy of the intersubband plasmon, as derived from the absorption experiments (triangles) and Eq. (2) (dashed line). (b) Polaritons frequencies ω_{UP} and ω_{LP} as a function of the cavity frequency ω_c. The dots are experimental results, and the continuous lines are the roots of Eq. (6) with $f_w = 0.62$ and $\omega_P = 1.8$ THz. The hatched zone indicates the polariton gap.

when $\hbar\omega_c = E_{12}$, while the (red) dashed line corresponds to the case $f_w = 0$. The agreement with the data, using no adjustable parameters, is excellent. Moreover, the strong deviation of the polariton curves from the linear approximation $\omega = \omega_{12} \pm \sqrt{f_w}\omega_P/2$ [red arrows in Fig. 4(a)], is unambiguous evidence of the ultrastrong coupling regime [8].

A relevant consequence of the large ratio $2\Omega_R/\omega_{12}$ is the opening of an energy gap ΔE_{gap} where no polaritonic solutions can be found. This is illustrated in the Fig. 4(b) where the polariton resonances are plotted as a function of the cavity frequency ω_c, both from the experiment and the roots of Eq. (6). The forbidden frequencies correspond to destructive interference between the electromagnetic field radiated by the electronic oscillations and the bare microcavity photon field. This is analogue to the case of the forbidden optical phonon band of bulk polar semiconductors [22]. The evidence of the forbidden band, $\Delta E_{\mathrm{gap}} \approx f_w\omega_P^2/2\omega_{12} = 2\Omega_R^2/\omega_{12}$ is another proof of the strength of the light-matter coupling. From our measurements we deduce $\Delta E_{\mathrm{gap}} = 330$ GHz, which is greater than the polariton linewidth (250 GHz). Such a gap has already been observed for bulk ($f_w = 1$) excitonic systems, but never for any microcavity-coupled electronic system, to our knowledge.

In conclusion, we have explored a 0D microcavity-coupled high density electronic system which has allowed us to reach the ultrastrong light-matter coupling regime. Our results, both theoretical and experimental, show that in this limit light-matter interaction is linked to the collective excitations of the electron gas, which yield the dominant nonlinearity in the polariton splitting. This occurs because for high electronic densities the energy exchanged by the electronic polarization with its own emitted field is a non-negligible effect. Theoretically, this is expressed by the weight of the quadratic term that, in the dipolar Hamiltonian, becomes comparable to the light-matter interaction one. We believe these results form the basis for quantum devices based on the ultrastrong light-matter coupling in the THz/μ-wave spectral range.

We thank L. Tosetto and H. Detz for technical help. We gratefully acknowledge support from the French National Research Agency through the program ANR-05-NANO-049 Interpol and from the Austrian Science Fund (FWF).

*yanko.todorov@univ-paris-diderot.fr

[1] Y. Yamamoto, F. Tassone, and C. Cao, *Semiconductor Cavity Quantum Electrodynamics* (Springer-Verlag, Berlin, 2000).
[2] L. Adreani, in *Proceedings of the International School of Physics Enrico Fermi, Course CL*, edited by B. Deveaud, A. Quattropani, and P. Schwendimann (IOS Press, Amsterdam, 2003).
[3] J. J. Hopfield, Phys. Rev. **112**, 1555 (1958).
[4] M. Artoni and J. L. Birman, Phys. Rev. B **44**, 3736 (1991).
[5] D. Dini, R. Kohler, A. Tredicucci, G. Biasiol, and L. Sorba, Phys. Rev. Lett. **90**, 116401 (2003).
[6] Y. Todorov *et al.*, Phys. Rev. Lett. **102**, 186402 (2009).
[7] G. Günter *et al.*, Nature (London) **458**, 178 (2009).
[8] C. Ciuti, G. Bastard, and I. Carusotto, Phys. Rev. B **72**, 115303 (2005).
[9] T. Ando, A. B. Fowler, and F. Stern, Rev. Mod. Phys. **54**, 437 (1982).
[10] T. Niemczyk *et al.*, Nature Phys. **6**, 772 (2010).
[11] C. Cohen-Tanoudji, J. Dupont-Roc, and G. Grynberg, *Photons and atoms: Introduction to the Quantum Electrodynamics* (CNRS Editions, Paris, 2001).
[12] L. Knöll, S. Scheel, and D.-G. Welsch, *QED in Dispersing and Absorbing Media*, in Coherence and Statistics of Photons and Atoms, edited by J. Perina (Wiley, New York, 2001).
[13] H. Haug and S. W. Koch, *Quantum Theory of the Optical and Electronic Properties of Semiconductors* (World Scientific, Singapore, 2004), 4th ed..
[14] O. Di Stefano, S. Savasta, and R. Girlanda, Phys. Rev. A **60**, 1614 (1999).
[15] Y. Todorov *et al.*, Opt. Express **18**, 13 886 (2010).
[16] K. Kakazu and Y. S. Kim, Phys. Rev. A **50**, 1830 (1994).
[17] F. Schwabl, *Advanced Quantum Mechanics* (Springer, Berlin 1997).
[18] M. Helm in *Intersubband Transitions in Quantum Wells: Physics and Device Applications I*, edited by H. C. Liu and F. Capasso (Academic Press, San Diego, 2000).
[19] See supplementary material at http://link.aps.org/supplemental/10.1103/PhysRevLett.105.196402 for this transformation.
[20] L. Wendler and T. Kraft, Phys. Rev. B **54**, 11 436 (1996).
[21] M. Zaluzny and C. Nalewajko, Phys. Rev. B **59**, 13 043 (1999).
[22] C. Kittel, *Quantum Theory of Solids* (John Wiley & Sons, New York, 1963).